CIRCRES/2016/310277 R2

Supplemental Material

Myocardial tissue engineering with cardiac cells derived from human induced-pluripotent stem cells and a native-like, high-resolution, 3-dimensionally printed scaffold

Ling Gao[1], Molly E. Kupfer[2], Jangwook P. Jung[2], Libang Yang[2], Patrick Zhang[2], Yong Da Sie[3], Quyen Tran[3], Visar Ajeti[3], Brian T. Freeman[2], Vladimir G. Fast[1], Paul J. Campagnola[3], Brenda M. Ogle[2]*, Jianyi Zhang[1]*

[1] Department of Biomedical Engineering, School of Medicine, School of Engineering, University of Alabama at Birmingham; [2] Department of Biomedical Engineering, University of Minnesota – Twin Cities, Minneapolis, MN 555455 USA; [3] Department of Biomedical Engineering, University of Wisconsin – Madison, Madison, WI 53706 USA

Short title: Gao, 3D-printed scaffolds for engineered myocardium

***Addresses for correspondence**

Dr. Jianyi Zhang, Department of Biomedical Engineering, School of Medicine, School of Engineering, University of Alabama at Birmingham, Birmingham, AL 35233 205-934-8421, E-mail: jayzhang@uab.edu

Dr. Brenda M. Ogle, Department of Biomedical Engineering, College of Science and Engineering, University of Minnesota – Twin Cities, Minneapolis, MN, 55455, 612-624-5948, E-mail: ogle@umn.edu

SUPPLEMENTARY METHODS

Creation of the ECM scaffold via 3D-MPE printing

Methacrylated gelatin (100 mg/mL) was mixed with sodium 4-[2-(4-morpholino)benzoyl-2-dimethylamino]-butylbenzenesulfonate (MBS) (1 mM) at 1% v/v, and crosslinking was performed on a glass slide, which served as the non-specific background. Two-photon excitation of the MBS photoactivator was induced with a 100 fs Ti:sapphire laser (Mira, Coherent, Santa Clara, CA) at 780 nm. A 10x, 0.5 NA objective lens was used, and the average power at the focus was kept constant (~100 mW at 78 MHz repetition rate). Upon UV absorption, MBS degrades to benzoyl and an α-aminoalkyl radical, which then attack residues containing aromatic groups and free amines[1]; then, the radical protein links to a second protein molecule, generating a covalent bond.

Our custom-built multiphoton instrument, which has been described in detail previously, [2] can produce scaffolds with more complexity and in a greater variety of sizes than can be achieved with a commercial laser-scanning microscope. The Ti:sapphire laser is coupled to a upright microscope stand (Axioskop 2, Zeiss, Thornewood, NY), and scanning is performed by combining a laser-scanning galvos (Cambridge Technolgoies, Bedford, MA) with a motorized stage (x-y-z, Ludl Electronic Products Ltd, Hawthorne, NY). The apparatus is controlled with LabVIEW software, and data is acquired with a field-programmable gate array (FPGA) board (Virtex-II PCI-7831R, National Instruments, Austin, TX).[2] The laser power entering the optical train is regulated with a 10 kHz electro-optic modulator (EOM) (Conoptics, Danbuty, CT), and the laser is rapidly shuttered with a second, higher-speed EOM (maximum 100 MHz; Conoptics). Parameters such as power, scanning area, the scan rate of the galvanometer, and repetition of the scanning pattern (i.e., the number of scans per layer) are set via a graphical user interface (GUI), while the TPEF of the entrapped residual photoactivator

serves as the online diagnostic signal for crosslinking and is read by the FPGA. The microscope is also equipped with phase-contrast and two-photon fluorescence imaging capabilities for characterizing the scaffold (e.g. immunofluorescence and quality control), and the minimum size of the features in the crosslinked protein structure corresponds to the two-photon excited point spread function (PSF). For example, when using 0.75 NA and 780 nm two-photon excitation, the lateral and axial resolution are about 600 nm and 1.8 μm, respectively[2, 3] MPE polymerization can also produce features with sub-micron resolution, because of chemical nonlinearity in the free radical kinetics,[3] but this does not occur during the crosslinking of proteins.

The FPGA was incorporated into the system to exploit the parallelism of command executions (80 MHz clock rate) and to avoid bottlenecks in communication between the CPU and the hardware, which occurs through four first in, first out (FIFO) channels. Two FIFO channels relay information from the main LabVIEW program to the FPGA for control of the galvanometer mirrors and fast EOM shutter, while the other two record information from the PMT to create an image of the fabrication; thus, communication between the CPU and hardware occurs in near real-time. The source code of the instrument control software is freely available at: http://campagnola.molbio.wisc.edu/.

The scanning approach (i.e., “modulated raster scanning”) combines the advantages of both raster scanning and vector scanning.[4] The galvanometers are raster scanned at maximum speed (~40 kHz), while the laser is shuttered at an even greater rate (10 MHz-40kHz) with the fast EOM. This approach is more accurate than modulating the scanning speed and/or step size of the galvanometers, because it is run over the whole field of view at constant speed and with the same pulse energy and repetition rate. The average power entering the fast-shuttering EOM is set by the slower EOM, which allows the entire scanning process to be performed at constant peak power and, consequently,

the fractional “on-time” within each pixel defines the integrated exposure dose, which is a linear process that directly correlates to the resulting protein concentration. Thus, we achieve a linear map between the intensity in the original image data and the fabricated structure.

Fabrication was based on 8-bit, 3D image files (.bmp or .tif) that were acquired with sampling that satisfied the Nyquist criterion, which is crucial for ensuring that the tissue is accurately represented and that the resolution (i.e., the sizes of the features) matches that of the original image, as well as for optimizing the structural integrity of the fabricated scaffold in 3D. Fabrication proceeded through the image stack via a Z-step pattern, and upon completion, the fidelity of the structure to the image stack was measured by using FIJI software to compare, pixel-by-pixel, the gray-scale intensity of the original (or processed) image to the two-photon excited fluorescence image of the fabricated construct.

Generation and characterization of hciPSC-derived cardiac cells

Recent reports from our laboratory suggest that the cells derived from induced-pluripotent stem cells (iPSCs) may be more effective for treatment of myocardial injury, and that the Ca^{2+} handling profile of iPSC-derived CMs is more cardiac-like, if the iPSCs are reprogrammed from cardiac, rather than dermal, fibroblasts.[5, 6] Thus, the CMs, SMCs, and ECs used in this study were generated from human, cardiac-lineage, iPSCs (hciPSCs), which had been reprogrammed from male, human, cardiac fibroblasts by transfecting the cells with lentiviruses coding for OCT4, SOX2, KLF4, and C-MYC.[5] After reprogramming, the hciPSCs were engineered to constitutively express green fluorescent protein (GFP), cultured in Matrigel-coated plate with human iPSC growth medium, and regularly passaged every 6-7 days.

hciPSCs were differentiated into ECs and SMCs as described previously.[7, 8] Briefly, the undifferentiated cells were treated with a GSK-3β inhibitor and ascorbic acid to induce mesoderm differentiation. Five days later, cells that expressed CD34 (i.e., hciPSC-derived vascular progenitor cells [hciPSC-VPCs]) were collected via magnetic nanoparticle selection; then, the hciPSC-VCs were differentiated into ECs by culturing them on fibronectin-coated flasks with EC-developmental medium (EGM2-MV; Lonza, Basel, Switzerland) or into SMCs by culturing them on collagen IV-coated flasks with SMC-developmental medium (SmGM-2; Lonza) containing PDGF-BB and TGF-β. ECs were purified to >95% via flow-cytometry selection for both CD31 and CD144 expression and then characterized via the expression of CD31, CD144, and von Willebrand factor-8 (vWF-8). SMCs were characterized via the expression of α smooth-muscle actin (αSMA), smooth-muscle 22 alpha (SM22), and calponin.

hciPSCs were differentiated into CMs as previously reported.[9] Briefly, the undifferentiated cells were expanded on a Matrigel®-coated dish for 4 days; then, differentiation was induced on day 0 by culturing the cells with a GSK-3β inhibitor in RPMI basal medium plus B27 without insulin (B27$^-$). The cells were recovered 24 hours later, cultured in RPMI basal medium plus B27$^-$ for 2 days, and then cultured in RPMI basal medium plus B27$^-$ and a Wnt signaling inhibitor; beating cells usually appeared about 8 days after differentiation was initiated. The hciPSC-CMs were purified to >95% via metabolic selection[10] and characterized via the expression of cardiac troponin I (cTnI), cardiac troponin T (cTnT), α-sarcomeric actin (αSA), Connexin 43, and ventricular myosin light chain-2 (MLC-2v).

Creation of the human iPSC-derived cardiac muscle patchs (hCMPs) and control patches

The hCMPs (2 mm × 2 mm, 100 μm thick) were created by combining the

3D-MPE–fabricated scaffold with a 2:1:1 ratio of hciPSC-CMs, hciPSC-ECs, and hciPSC-SMCs. A total of ~50,000 cells (i.e., 12,500 cells/mm^2) were seeded onto the surface of the scaffold; then, the hCMPs were cultured in Dulbecco minimum essential medium (DMEM) with 10% fetal calf serum for 1 week before *in vitro* analyses were performed or for 1 day before *in vivo* transplantation. For the *in-vitro* experiments, control patches were created by combining the same density and ratio of hciPSC-CMs, -ECs, and -SMCs with a chemoselectively cross-linked polyethylene glycol (PEG) gel[11] or with decellularized bovine pericardium; the control patches were also cultured in DMEM with 10% fetal calf serum for 1 week.

Measurement of calcium transients

hCMPs were loaded with 5 µM Fluo-4 AM (Life Technologies, USA) and incubated at 37°C and 5% CO_2 for 30 min; then, the intercellular AM esters were de-esterified by incubating the hCMPs with Tyrode's salt solution at 37°C and 5% CO_2 for another 30 min. Intracellular calcium transients were recorded with a Zeiss Cell Observer Spinning Disk Confocal microscope equipped with a 20X (NA = 0.5) objective and an environmental chamber (37°C, 5% CO_2) over 30 to 120 s. Movies were analyzed with FIJI software to measure the fluorescence intensities for 2 to 8 regions of interest (F) and for 3 to 8 background regions (F_0) per acquisition.

***In vitro* analysis of contractility**

Videos of the beating hCMPs were taken at 24 fps; then, the speed of contraction and relaxation, as well as the peak beat rate, of the hCMP was determined with motion vector analysis software developed by Huebsch, *et al.*[12]

Optical mapping of activation

hCMPs were transferred to a perfusion chamber mounted on an inverted microscope

and perfused with Hank's balanced salt solution at 37^{o}C. Preparations were stimulated with 2-ms rectangular pulses delivered from a bipolar electrode. Cells were stained with V_m-sensitive dye RH-237 (5 μM) for 5 min. To eliminate motion artifact from optical recordings, cell contractions were inhibited by supplementing staining and perfusion solutions with 10 μM of blebbistatin. Dye fluorescence was excited using an Hg/Xe arc lamp and a 560/55-nm excitation filter and measured at >650 nm using a 16x16 photodiode array at spatial resolution of 110 μm per diode, as previously described.[13]

Optical signals were digitally filtered to increase the signal-to-noise ratio. Activation times were measured at the 50% level of action potential amplitude and used to construct the isochronal maps of activation spread. Conduction velocity was calculated at each recording site from local activation times and averaged across the whole map using custom-written data analysis software. Action potential durations were measured at 50% and 80% levels of repolarization (APD_{50} and APD_{80}, respectively) as intervals between repolarization and activation times.

Cardiac monolayer culture

Cell suspensions containing a 2:1:1 ratio of hciPSC-CMs, -ECs, and -SMCs were seeded on a gelatin coated plate at a density of $1.2x10^5$ cells/cm^2 and cultured in DMEM with 10% fetal calf serum; the culture media was changed every 2 days.

Quantitative RT-PCR Analysis

Total RNA was extracted by using Qiashredder and RNeasy mini kits (Qiagen, USA) as directed by the manufacturer's instructions; then, the RNA (1-2 μg per 20 μL reaction) was reverse transcribed with SuperScript™ II Reverse Transcriptase (Thermo Scientific, USA) and appropriate primers (Supplemental Table 1). Quantitative PCR was performed with Maxima SYBR Green Master Mix (Thermo Scientific) on a Realplex^2 Real-Time

PCR system (Eppendorf, USA). Measurements were calculated via the 2−ΔCt method and normalized to glyceraldehyde phosphate dehydrogenase RNA levels.

Murine model of myocardial infarction and hCMP administration

All experimental procedures that involved animals were approved by the Institutional Animal Care and Use Committee of the University of Minnesota, performed in accordance with the Animal Use Guidelines of the University of Minnesota, and consistent with the National Institutes of Health Guide for the Care and Use of Laboratory Animals (NIH publication No 85-23). Twelve-week-old immunodeficient NOD-scid/γc$^{-/-}$ mice (Jackson Laboratory) were anesthetized with an intraperitoneal injection of sodium pentobarbital (35 mg/kg), intubated, and ventilated with a small animal respirator (Harvard Apparatus); then, a left thoracotomy was performed to expose the heart, and the left-anterior descending coronary artery was permanently ligated with an 8.0 surgical silk suture. Fifteen minutes after ligation, animals in the MI+hCMP group were treated with two hCMPs, and animals in the MI+Scaffold group were treated with two 3D-MPE–printed scaffolds that lacked any cells. Both treatments were applied to the epicardial surface over the infarcted area—the hCMP was oriented approximately parallel to the alignment of the surface myocardium and held in place by covering them with a piece of decellularized bovine pericardium that was sutured to the heart to avoid movement of hCMPs off the heart and prevent adhesions between the heart and the rib cage. Both the hCMP and the cell-free scaffold were withheld from animals in the MI group, and animals in the Sham group underwent all surgical procedures for MI induction except the ligation step and received neither of the experimental treatments. The chest was closed in layers and the animals were allowed to recover.

Echocardiographic assessments of cardiac function

Echocardiographic measurements were obtained via the method recommended by the

American Society of Echocardiography and performed on a Vevo770 Imaging System equipped with an RMV 707B transducer (15-45MH; VisualSonics Inc, Canada); both conventional 2-dimensional images and M-Mode images of the heart in a parasternal short axis view were acquired. Left ventricular (LV) internal diameters at end-diastole (LVIDed) and end-systole (LVIDes) were determined from 8 consecutive images, and LV ejection fractions (EF) and fractional shortening (FS) were calculated according to the following equations:

$EF=(LVIDed^3-LVIDes^3)/LVIDed^3\times100\%$；$FS=(LVIDed-LVIDes)/LVIDed\times100\%$.

Immunohistochemical evaluations

The hCMPs were fixed with 4% paraformaldehyde for 20 min, permeabilized with 0.2% Triton X-100 for 15 min, and then blocked with 5% donkey serum for 30 min. Primary antibodies (rabbit anti-cTnI [Abcam, USA], mouse anti-cTnT [Thermo Scientific, USA], mouse anti-αSMA [Sigma-Aldrich, USA], and goat anti-CD31 [Santa Cruz, USA]) were diluted in the blocking solution, and the hCMPs were incubated at 4°C; on the following day, the hCMPs were incubated with secondary antibodies for 1 h and then stained with DAPI. The alignment of cells in the hCMP channels was evaluated via multiphoton microscopy. ImageJ software was used to fit an ellipse to the outline of each cell, which was visible because of cellular autofluorescence, and the ellipse was used to determine the cell's aspect ratio and angle relative to horizontal; then, the angle of orientation for each cell was normalized to the average longitudinal angle of the channel walls.

Murine hearts were cut into halves from the middle of the infarct. One of the halves was frozen at the optimal cutting temperature for cryo-sectioning, and the other half was stored in 10% formalin for paraffin-embedded sectioning. Embedded tissues were cut into 7-μm sections; then, the sections were fixed with 4% paraformaldehyde for 20 min at room temperature, permeabilized in 0.1% Triton X-100 at 4ºC for 10 min, and blocked

with UltraV block (Thermo Scientific, USA) for 7 min. Primary antibodies (mouse anti-human specifc nuclear antigen, HNA [Emdmillipore, USA], goat anti-GFP [Abcam, USA], goat anti-CD31 [Santa Cruz, USA], mouse anti-human specific CD31 [hCD31, Dako, USA], mouse anti-αSMA [Sigma-Aldrich, USA], rabbit anti-cTnI [Abcam, USA], mouse anti-cTnT [Abcam, USA], rabbit anti-Ki67 [Abcam, USA]) were added to the UltraV block buffer, and the sections were incubated at 4ºC. On the following day, secondary antibodies conjugated with fluorescent markers (Jackson ImmunoResearch Lab, USA) were added; then, the sections were incubated for 1 h at room temperature, stained with DAPI, washed, and examined under a confocal microscope (Zeiss 710, USA).

Engrafted hciPSC-cardiovascular cells were identified by the expression of HNA or GFP, engrafted hciPSC-CMs were identified by the expression of both GFP and cTnI, or both HNA and cTnI, engrafted hiPSC-ECs were identified by hCD31 expression, and engrafted hiPSC-SMCs were identified by the expression of both GFP and αSMA. Vascular density was evaluated by counting the number of vascular structures that were positive for either CD31 or αSMA expression; then, the images used for the CD31 and αSMA evaluations were superimposed, and arteriole density was evaluated by counting the number of structures that expressed both CD31 and αSMA. Cells and vessels were counted in 5 fields per section, 5 sections per animal.

Engraftment rate assessment

Engraftment rates were evaluated via quantitative PCR (qPCR) assessments of the human Y-chromosome as previous reported.[14] Briefly, whole hearts of female mice were collected and digested overnight at 56 ^{o}C with proteinase K; then, the total DNA was isolated from the digested buffer with a QIAGEN DNA isolation kit. The number of cells in each mouse heart was determined by comparing the number of cycles required for each

sample to a standard curve calculated from the DNA of known quantities of undifferentiated hciPSCs, and the engraftment rate was calculated as the number of cells in each animal divided by the number of cells administered ($1x10^5$). Analyses were performed with the SYBR Green kit (Thermo Scientific, USA) on an Eppendorf Realplex^2 PCR system (Eppendorf, USA) with the following primers: sense, ATCAGCCTAGCCTGTCTT-CAGCAA; anti-sense, TTCACGACCAACAGCACAGCAATG.

To assess the engraftment rate by counting the grafted human cells as evidenced by HNA positivity, we also used histologic assessment of consecutives sections of the heart that spans the entire area covered by the engrafted patch, and counting the grafted human cells as evidenced by HNA positivity. [5, 15] Hearts were frozen or paraffin-embedded and transversely cut into 7-µm sections from base to apex. Total cell nuclei were stained with 4,6-diamidino-2-phenylindole (DAPI). Engrafted hciPSCs-derived cardiovascular cells were identified by counting the human specific nuclear antigen (HNA)-positive cells in every 15th serial section of the heart and then multiplying by 15 to obtain the total number of engrafted hciPSC-cardiovascular cells per heart. The engraftment rate of transplanted hciPSC-cardiovascular cells was calculated by dividing the total number of engrafted cells by the number of cells administered ($1x10^5$) and multiplying by 100.

Infarct size and thickness measurements

Hearts were frozen or paraffin-embedded and cut into 7-µm sections; then, the sections were stained with an Accustain Trichrome Stains (Masson) kit (Sigma-Aldrich, USA). The infarct size was measured from Masson's trichrome-stained sections as the percentage of the surface area of the left ventricular anterior wall occupied by scar, and infarct thickness was calculated as the ratio of the thicknesses of the fibrous region to the thickness of the septal wall. For each heart, the infarct size was averaged from three areas of the heart: just below the ligation suture, midway between the ligation suture and

the apex, and a section close to the apex.

Apoptosis

Sections cut from embedded hearts were TUNEL stained with an In-situ Cell Death Detection Kit (Roche Applied Science, Germany) and viewed at 40x magnification as previously reported.[5] The number of TUNEL-positive cells and the total number of cells were counted in 5 to 6 slides per animal and 5 fields per slide.

Statistical Analyses

Data are presented as mean ± standard error. Statistical significance ($P<0.05$) between two experimental groups was determined via the Student's two-tailed *t*-test, assuming unequal variance. Comparisons among more than two experimental groups were evaluated via one-way ANOVA followed by Tukey post-hoc analysis. All statistical analyses were performed with SPSS software (version 13.0, SPSS, USA).

SUPPLEMENTAL REFERENCES

1. Kojima K, Masato I, Morishita H and Hayashi N. A novel water-soluble photoinitiator for the acrylic photopolymerization type resist system. *Chem Mater*. 1998;10:3429-3433.
2. Sridhar M, Basu S, Scranton VL and Campagnola PJ. Construction of a laser scanning microscope for multiphoton excited optical fabrication. *Rev Sci Instrum*. 2003;74:3474-3477.
3. Maruoka N, Murata T, Omata N, Takashima Y, Fujibayashi Y and Wada Y. Effects of vitamin E supplementation on plasma membrane permeabilization and fluidization induced by chlorpromazine in the rat brain. *J Psychopharmacol*. 2008;22:119-27.
4. Ajeti V, Lien CH, Chen SJ, Su PJ, Squirrell JM, Molinarolo KH, Lyons GE, Eliceiri KW, Ogle BM and Campagnola PJ. Image-inspired 3D multiphoton excited fabrication of extracellular matrix structures by modulated raster scanning. *Opt Express*. 2013;21:25346-55.
5. Zhang L, Guo J, Zhang P, Xiong Q, Wu SC, Xia L, Roy SS, Tolar J, O'Connell TD, Kyba M, Liao K and Zhang J. Derivation and high engraftment of patient-specific cardiomyocyte sheet using induced pluripotent stem cells generated from adult cardiac fibroblast. *Circ Heart Fail*. 2015;8:156-66.
6. Zhang X, Shen MR, Xu ZD, Hu Z, Chen C, Chi YL, Kong ZD, Li ZF, Li XT, Guo SL, Xiong SH and Zhang CS. Cardiomyocyte differentiation induced in cardiac progenitor cells by cardiac fibroblast-conditioned medium. *Exp Biol Med (Maywood)*. 2014;239:628-37.
7. Lian X, Bao X, Al-Ahmad A, Liu J, Wu Y, Dong W, Dunn KK, Shusta EV and Palecek SP. Efficient differentiation of human pluripotent stem cells to endothelial progenitors via small-molecule activation of WNT signaling. *Stem Cell Reports*. 2014;3:804-16.
8. Bao X, Lian X, Dunn KK, Shi M, Han T, Qian T, Bhute VJ, Canfield SG and Palecek SP. Chemically-defined albumin-free differentiation of human pluripotent stem cells

to endothelial progenitor cells. *Stem Cell Res*. 2015;15:122-9.

9. Lian X, Zhang J, Azarin SM, Zhu K, Hazeltine LB, Bao X, Hsiao C, Kamp TJ and Palecek SP. Directed cardiomyocyte differentiation from human pluripotent stem cells by modulating Wnt/beta-catenin signaling under fully defined conditions. *Nat Protoc*. 2013;8:162-75.
10. Tohyama S, Hattori F, Sano M, Hishiki T, Nagahata Y, Matsuura T, Hashimoto H, Suzuki T, Yamashita H, Satoh Y, Egashira T, Seki T, Muraoka N, Yamakawa H, Ohgino Y, Tanaka T, Yoichi M, Yuasa S, Murata M, Suematsu M and Fukuda K. Distinct metabolic flow enables large-scale purification of mouse and human pluripotent stem cell-derived cardiomyocytes. *Cell Stem Cell*. 2013;12:127-37.
11. Jung JP, Sprangers AJ, Byce JR, Su J, Squirrell JM, Messersmith PB, Eliceiri KW and Ogle BM. ECM-incorporated hydrogels cross-linked via native chemical ligation to engineer stem cell microenvironments. *Biomacromolecules*. 2013;14:3102-11.
12. Huebsch N, Loskill P, Mandegar MA, Marks NC, Sheehan AS, Ma Z, Mathur A, Nguyen TN, Yoo JC, Judge LM, Spencer CI, Chukka AC, Russell CR, So PL, Conklin BR and Healy KE. Automated Video-Based Analysis of Contractility and Calcium Flux in Human-Induced Pluripotent Stem Cell-Derived Cardiomyocytes Cultured over Different Spatial Scales. *Tissue Eng Part C Methods*. 2015;21:467-79.
13. Sowell B and Fast VG. Ionic mechanism of shock-induced arrhythmias: role of intracellular calcium. *Heart rhythm : the official journal of the Heart Rhythm Society*. 2012;9:96-104.
14. Ye L, Chang YH, Xiong Q, Zhang P, Zhang L, Somasundaram P, Lepley M, Swingen C, Su L, Wendel JS, Guo J, Jang A, Rosenbush D, Greder L, Dutton JR, Zhang J, Kamp TJ, Kaufman DS, Ge Y and Zhang J. Cardiac repair in a porcine model of acute myocardial infarction with human induced pluripotent stem cell-derived cardiovascular cells. *Cell stem cell*. 2014;15:750-61.
15. Nakamura Y, Wang X, Xu C, Asakura A, Yoshiyama M, From AH and Zhang J.

Xenotransplantation of Long Term Cultured Swine Bone Marrow-Derived Mesenchymal Stem Cells. *Stem Cells*. 2006.

ONLINE FIGURE LEGENDS

Online Figure I. Immunofluorescent analysis of lineage-specific marker expression in differentiated hiPSC-derived cardiac cells. The lineage of the differentiated hciPSC-CMs was confirmed via the expression of cardiac troponin I (cTnI), cardiac troponin T (cTnT), ventricular myosin light chain 2 (MLC-2v), α-sarcomeric actin (αSA), and the gap-junction protein connexin-43 (Con-43); the lineage of the differentiated hciPSC-SMCs was confirmed via the expression of α-smooth muscle actin (αSMA), SM22, and calponin; and the lineage of the differentiated hciPSC-ECs was confirmed via the expression of CD31, CD144, and von Villebrand factor 8 (vWF-8). Nuclei were counterstained with DAPI (scale bar = 50 μm).

Online Figure II. Expression of contractile- and calcium-transient–related genes in hCMPs and in monolayers of hiPSC-derived cardiac cells. Quantitative PCR measurements of the expression of genes involved in (**A**) contractile activity (cTnT, cTnI, atrial myosin light chain 2 [MLC2a], MLC2v, α myosin heavy chain [αMHC], βMHC), and (**B**) generating calcium transients (sarcoplasmic reticulum Ca^{2+}-ATPase 2 α [SERCA2α], phospholamban [PLB], sodium/calcium exchanger 1 [NCX1], ryanodine receptor 2 [RYR2], calsequestrin 2 [CASQ2]) were performed in hCMPs and in monolayers composed of equivalent populations of cells on day 1 and day 7 after manufacture. Results were normalized to measurements obtained in monolayers on day 1. **P*<0.05, ***P*<0.01; n=3-4 hCMPs or monolayers per time point with 3 replicates per measurement.

Online Figure III. hCMP transplantation reduces apoptosis and increases angiogenesis after MI. (**A**) Apoptotic cells were identified in sections from the border-zone of ischemia in the hearts of animals from the MI (top row), MI+Scaffold (middle row), and MI+hCMP (bottom row) groups via TUNEL staining; CMs were

visualized via immunofluorescent staining for the presence of cTnI and nuclei were counterstained with DAPI. (**B**) Apoptosis was quantified as the percentage of cells that were positive for TUNEL staining. (**C**) Sections from the border-zone of ischemia in the hearts of MI (top row), MI+Scaffold (middle row), and MI+hCMP (bottom row) animals were immunofluorescently stained for the presence of the CD31, αSMA, and cTnI, and nuclei were counterstained with DAPI; then (**D**) vascular density was determined by quantifying the expression of CD31, and (**E**) arteriole density was determined by quantifying the co-expression of CD31 and αSMA. ***P*<0.01, n = 5-6 in each group; scale bar = 50 μm.

Online Figure IV. hCMP transplantation promotes cell proliferation after MI. (**A**) Proliferating cells were identified in sections from the border-zone of infarct in hearts on day 28 after MI by staining for expression of the proliferation marker Ki67 (green). (**B**) Proliferation was quantified as the number of $Ki67^+$ cells per high-power field (HPF). **P*<0.05, ***P*<0.01, n=5-6 in each group. Scale bar = 100 μm.

ONLINE VIDEO LEGENDS

Online Video I. MPE-3DP to fabricate adult simulate grid layer by layer. The video shows layer-by-layer fabrication of a scaffold of dimensions 400 x 400 x 100 microns. This is the same structure as was used for the *in vitro* experiments. For *in vivo* studies, structures like the one shown here were tiled together to generate millimeter scale structures. Fabrication of each layer required approximately 10 seconds. The fluorescent contrast arises from the two-photon excitation of Rose Bengal entrapped in the matrix.

Online Video II. 360 view of 3D rendering of adult simulate grid. The video shows a 3D projection of the series of fabricated layers shown in the S1 video, with a 360 view of the fabricated structure.

Online Video III. Animation depicting the MPE-3DP process. First, a solution containing the polymer or protein of interest and associate photocrosslinking agent is added to the reservoir. The reservoir sits upon a slide on the stage of a multiphoton microscopy rig. The pulsed laser is actuated and raster scanned across the x-y plane of a given field of view. The dwell time of the laser at a given focal volume is dictated by the intensity of the digital template at a given x-y position. The longer the dwell time, the more crosslinking occurs and therefore a more stable structural feature is formed. The scan time is on the scale of microseconds for each focal volume, milliseconds for each x-y line and seconds for the entire raster (i.e., x-y plane). The animation shows a significantly slowed visual depiction of proteins of focal volumes undergoing polymerization on three different z planes. Not shown in the video is the digital template, which dictates the final form of the structure. As noted at the end of the animation, the final structure can be manipulated for use *in vitro* and *in vivo*.

Online Video IV. Spontaneous and synchronous contractile activity in a hCMP on

day 1 after fabrication (magnification: 100 x).

Online Video V. Spontaneous and synchronous contractile activity in a hCMP on day 3 after fabrication (magnification: 100 x).

Online Table I. Primers for quantitative RT-PCR

Standard Gene name	**Gene product**	**Forward**	**Reverse**	**Size bp**
GAPDH	GAPDH	TCGACAGTCAGCCGCATCTTCTTT	ACCAAATCCGTTGACTCCGACCTT	94
TNNI3	cTNI	CCTCACTGACCCTCCAAACG	GAGGTTCCCTAGCCGCATC	104
TNNT2	cTNT	TTCACCAAAGATCTGCTCCTCGCT	TTATTACTGGTGTGGAGTGGGTGTGG	165
MYH6	αMHC	CTCCGTGAAGGGATAACCAGG	TTCACAGTCACCGTCTTCCC	248
MYH7	ßMHC	ACCAACCTGTCCAAGTTCCG	TCATTCAAGCCCTTCGTGCC	131
MYL2	MLC 2v	ACATCATCACCCACGGAGAAGAGA	ATTGGAACATGGCCTCTGGATGGA	164
MYL7	MLC 2a	GGAGTTCAAAGAAGCCTTCAGC	AAAGAGCGTGAGGAAGACGG	178
ACTN2	α-actinin 2	CTTCTACCACGCTTTTGCGG	CCATTCCAAAAGCTCACTCGC	136
ATP2A2	SERCA 2α	TCACCTGTGAGAATTGACTGG	AGAAAGAGTGTGCAGCGGAT	149
CASQ2	calsequestrin 2	GTTGCCCGGGACAATACTGA	CTGTGACATTCACCACCCCA	142
PLN	Phospholamban	ACAGCTGCCAAGGCTACCTA	GCTTTTGACGTGCTTGTTGA	191
SLC8A1	NCX 1	CTGGAATTCGAGCTCTCCAC	ACATCTGGAGCTCGAGGAAA	108
RYR2	RYR 2	TTGGAAGTGGACTCCAAGAAA	CGAAGACGAGATCCAGTTCC	141

Online Figure I

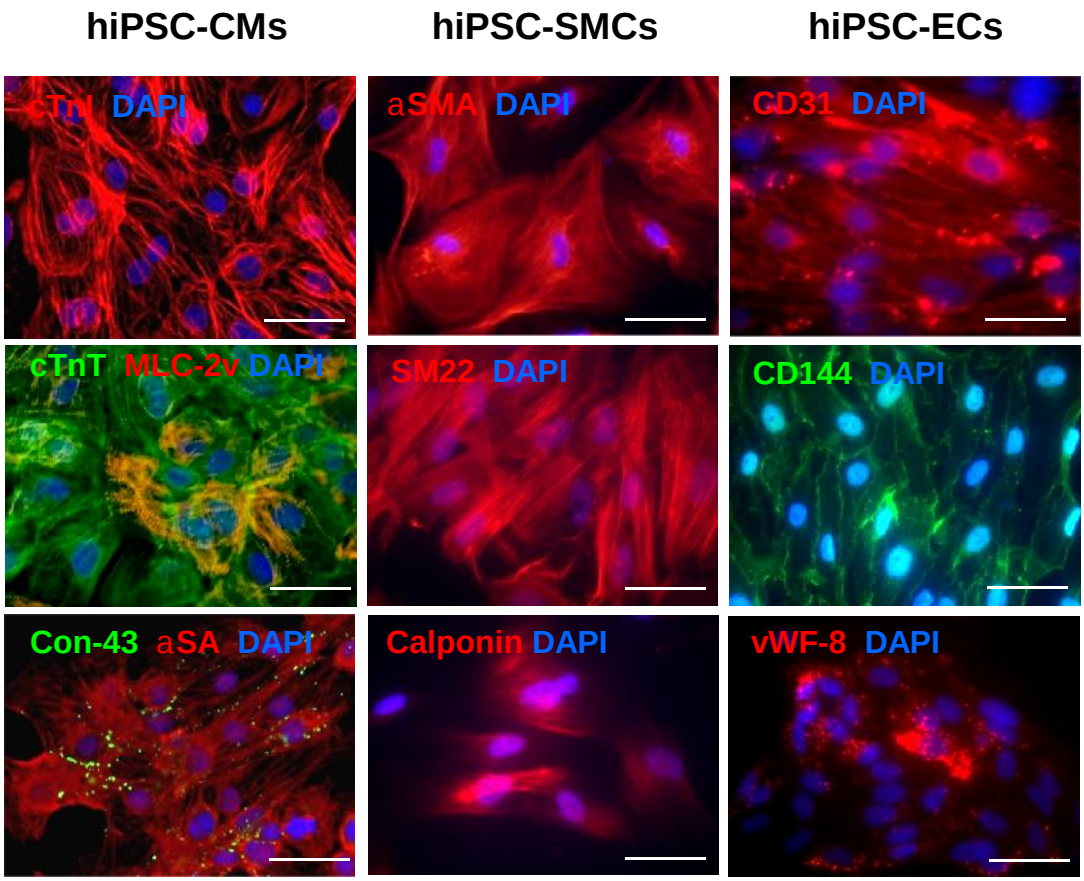

Online Figure II

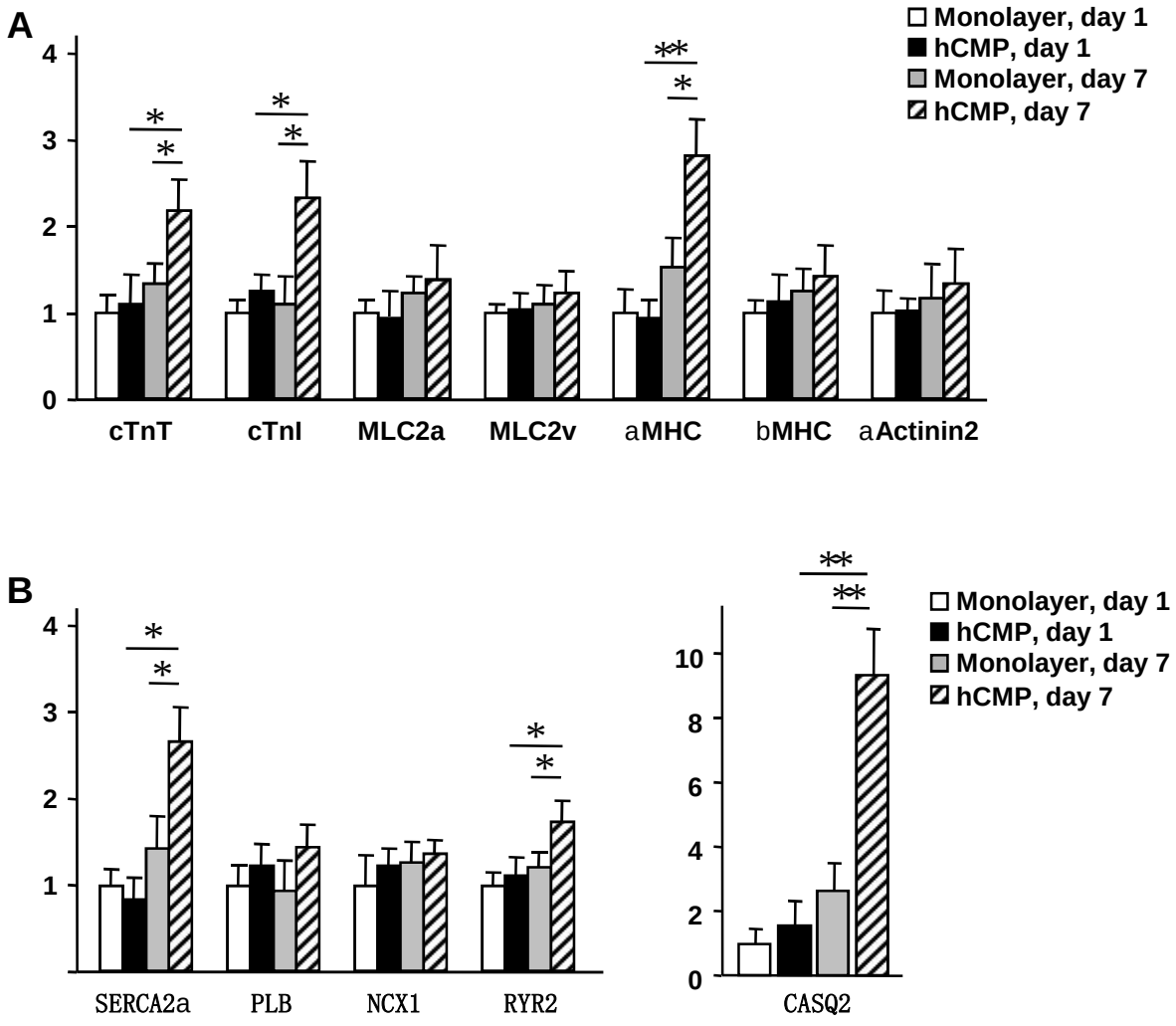

Online Figure III

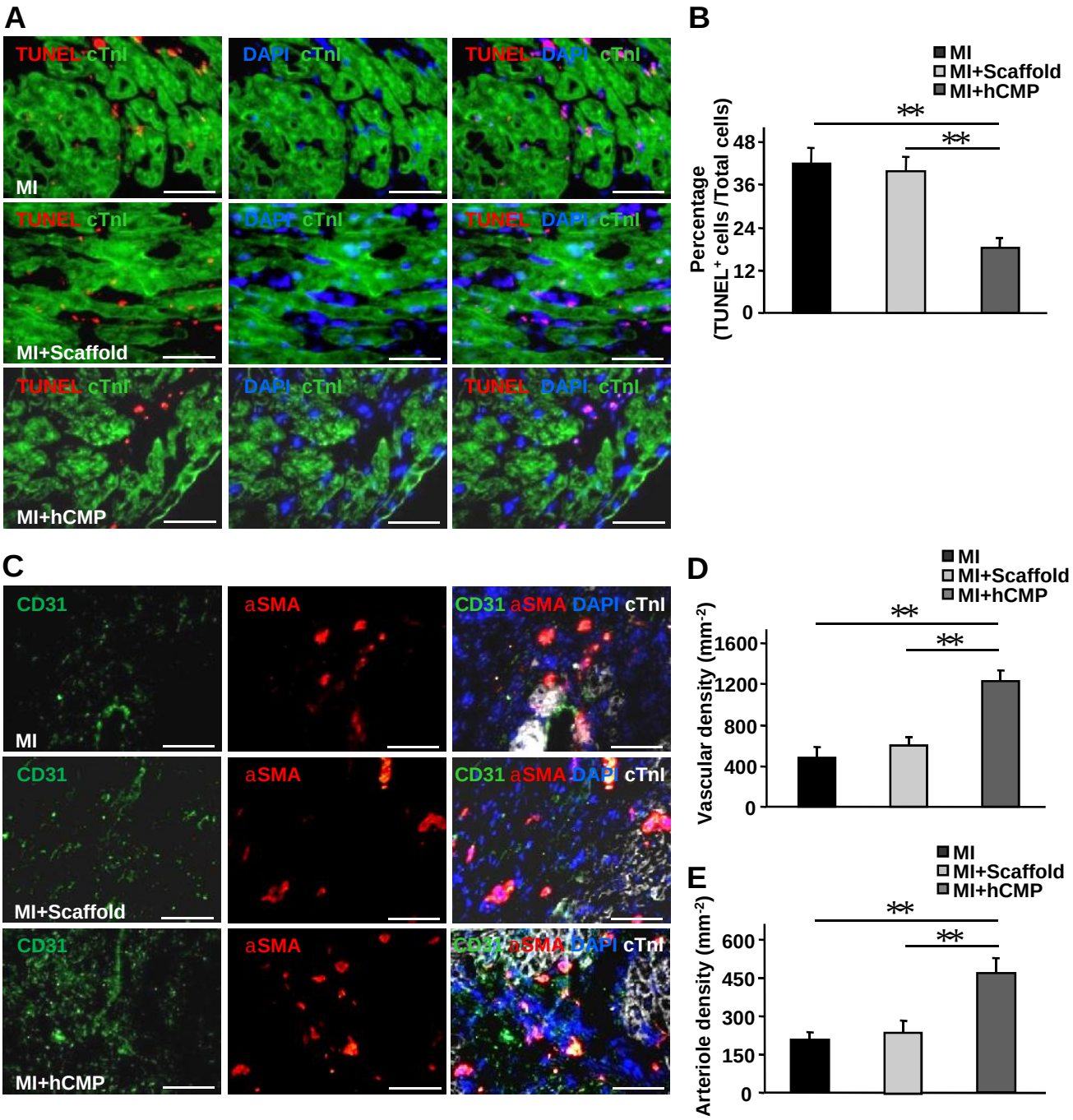

Online Figure IV